A numerical study of flow and heat transfer in internally finned rotating straight pipes and stationary curved pipes

M.R.H. Nobari *, K. Gharali

Amirkabir University of Technology, Mechanical Engineering Department, 424 Hafaz Ave., P.O. Box 15875-4413, Tehran, Iran

Abstract

In this article the effects of internal fins on laminar incompressible fluid flow and heat transfer inside rotating straight pipes and stationary curved pipes are numerically studied under hydrodynamically and thermally fully developed conditions. The fins are assumed to have negligible thickness with the same conditions as the pipe walls. Two cases, constant wall temperature and constant heat flux at the wall, are considered. First the accuracy of the numerical code written by a finite volume method based on SIMPLE algorithm is verified by the available data for the finless rotating straight pipes and stationary curved pipes, and then, the numerical results for those internally finned pipes are investigated in detail. The numerical results for different sizes and numbers of internal fins indicate that the flow and temperature field analogy between internally finned rotating straight pipes and stationary curved pipes still prevail. The effects of Dean number (K_L) versus friction factor, Nusselt number, and other non-dimensional parameters are studied in detail. From the numerical results obtained, an optimum fin height about 0.8 of pipe radius is determined for Dean numbers less than 100. At this optimum value, the heat transfer enhancement is maximum, and the heat transfer coefficient appears to be 6 times as that of corresponding finless pipes.
© 2005 Elsevier Ltd. All rights reserved.

Keywords: Curved pipe; Rotating straight pipe; Fully developed; Laminar flow

1. Introduction

One of the most common ways to increase the heat transfer coefficient and reduce the size of heat exchangers is the use of internal fins. By doing so, the flow friction and the pumping power will increase. However, the heat transfer enhancement dominates to drawback resulting from the increase of friction in an optimum thermal design. Compact heat exchangers, cooling systems of gas turbines, nuclear reactors, and jet engines are the examples among large number applications of internally finned tubes.

Many analytical, experimental, and numerical works regarding internally finned stationary straight pipes with different cross sectional areas were published. Among them, it can be referred briefly to the works of Nanda-

kumar and Masilyah [1] and Soliman et al. [2] in hydrodynamically fully developed flows, Soliman et al. [3], Masliyah and Nandhakumar [4], and Hu and Chang [5] in thermally fully developed flows, Rustum and Soliman [6] and Prakash and Liu [7] in thermally developing flows, Prakash and Patankar [8] in radial fin effects on the heat transfer enhancement, and Dong and Ebadian [9,10] in internal fin effects in a straight duct with elliptic cross section. Also within recent years Campo and Chang [11] have proposed correlations for friction factor and convective coefficients in tubes containing internally longitudinal fins, Fabbir [12] has investigated an optimum internal fin profile by a finite element method, Huq et al. [13] have studied experimentally heat transfer enhancement in an internally finned tube and indicated that heat transfer coefficient increases twice as much as finless pipes, Ledezma and Campo [14] have approximated Nusselt number distribution in entire length of the pipe by a simple approximate numerical method, Yu et al. [15] have studied experimentally the

Nomenclature

A_u	source term in r direction
A_v	source term in θ direction
A_w	source term in z or ϕ direction
C	pressure gradient in z direction
C_p	specific heat at constant pressure
d	pipe radius
F	friction coefficient
F_0	friction coefficient of finless stationary straight pipe
k	thermal conductivity
K_L	Dean number
K_{LC}	Dean number for curved pipe
K_{LR}	Dean number for rotating pipe
N	number of fins
N	unit normal vector
Nu	Nusselt number
Nu_T	Nusselt number at constant wall temperature
Nu_H	Nusselt number at constant heat flux at the wall
P	pressure
P^*	reduced pressure
Pr	Prandtl number
q_w	heat flux at the wall
r	radial coordinate
R	mean radius of curvature
T	fluid temperature
T_b	bulk fluid temperature

T_w	wall temperature
U	velocity in r direction
v	velocity in θ direction
w	axial velocity
w_m	mean axial velocity
z	axial coordinate

Greek symbols

α	thermal diffusivity
θ	angular coordinate
λ	ratio of mean radius of curvature to pipe diameter
Ω	angular velocity of rotation
ϕ	curvature coordinate
ρ	density
v	kinematic viscosity

Subscripts

0	finless stationary straight pipe
w	pipe wall
m	mean value
max	maximum value
b	bulk property

Superscript

$\sim$	dimensionless parameters

pressure drop and heat transfer enhancement in tubes with internal wave like longitudinal fins and offered correlations for friction factor and Nusselt number at the range of Reynolds numbers 900–3500. Tsui and Leu [16] have numerically studied the effect of vortex generator internal fins on heat transfer enhancement in three-dimensional case and declared that the heat transfer is greatly enhanced because of transport of the high speed core flow by the vortex to sweep across the wall and fins. Using Finite difference method, Sakalis and Hatzikonstantinou [17] have investigated laminar heat transfer in the internally finned square ducts and made a conclusion that in the thermally developing region heat transfer enhancement is high, but in thermally developed region as the fin height increases the heat transfer coefficient increases. Very recently, Zeitoun and Hegazy [18] have simulated numerically heat transfer in laminar flow of internally finned pipes with different fin heights at constant wall temperature. Their results indicate that using different fin heights causes the friction power to become less than that for the even fin height case. As it is clear from the above brief literature survey, all the investigations have considered different aspects of internal fin effects on the heat transfer enhancement in straight stationary pipes, and the simultaneous effect of internal fins and curvature/rotation on heat transfer coefficient is not considered to the best of our knowledge.

In this article, laminar incompressible flows in a rotating straight pipe and in a stationary curved pipe with internal longitudinal fins are studied numerically by a finite volume method. The flow is considered in hydrodynamically and thermally fully developed region, hence, the flow field, taking into account the symmetry, is simulated only in semi-circular cross section in both cases. The fins are assumed to have negligible thickness with a 100% efficiency. The effects of heat transfer enhancement in two different thermal boundary conditions, i.e. constant wall temperature and constant heat flux at the wall, are investigated. Also the analogy of flow field in the presence of internal fins between a rotating straight pipe and a stationary curved pipe is demonstrated. Finally, the optimum height of internal fins to have large amount of heat transfer enhancement without great increase of friction power is studied. It should be pointed out that to the best our knowledge, there have been no results reported for the flow in internally finned rotating straight and stationary curved pipes.

2. Governing equations

Here, two problems consisting of laminar incompressible viscous fluid flow in a stationary curved pipe and in a rotating straight pipe are studied in hydrodynamically and thermally fully developed conditions. The geometry
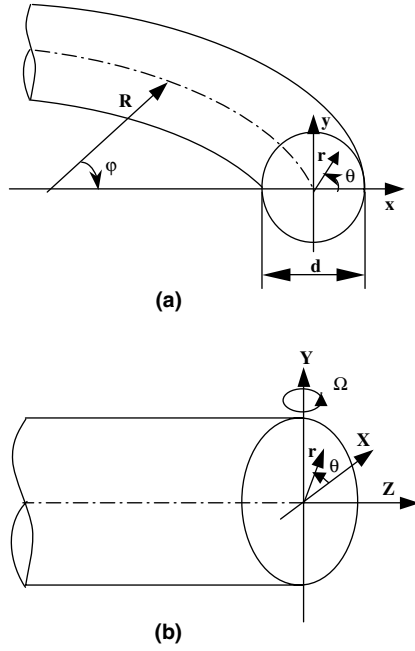
(a)

(b)

Fig. 1. Geometry of flow fields (a) curved pipe (b) rotating straight pipe.

of flow field for both cases involving pipes with circular cross section are shown in Fig. 1. The curved pipe is stationary with a mean radius of curvature R, and the straight pipe is rotating about an axis perpendicular to the main flow direction as in Fig. 1. For convenience the governing equations consisting of continuity, momentum, and energy equations are written in toroidal coordinates (r, θ, ϕ) for the stationary curved pipe and in cylindrical coordinates (r, θ, z) for the rotating straight pipe. To compact the equations, both cases are considered to follow the same equations with different source terms in each case. In the rotating straight pipe, the system of coordinate is rotational, and hence, the coriolis and centrifugal forces will appear in the momentum equations. It should be pointed out that for most applications the curvature radius of the curved pipe is much larger than the pipe radius, therefore, here, the loose coil approximation is applied. By taking into account the points mentioned above, the fully developed flow equations are as follows [19,20]:

$$\frac{\partial}{\partial r}(ru) + \frac{\partial v}{\partial \theta} = 0, \tag{1}$$

$$u\frac{\partial u}{\partial r} + \frac{v}{r}\frac{\partial u}{\partial \theta} - \frac{v^2}{r} + A_u$$
$$= \frac{-1}{\rho}\frac{\partial p^*}{\partial r} + v\left(\nabla^2 u - \frac{u}{r^2} - \frac{2}{r^2}\frac{\partial v}{\partial \theta}\right), \tag{2}$$

$$u\frac{\partial v}{\partial r} + \frac{v}{r}\frac{\partial v}{\partial \theta} + \frac{uv}{r} + A_v$$
$$= \frac{-1}{\rho r}\frac{\partial p^*}{\partial \theta} + v\left(\nabla^2 v - \frac{v}{r^2} + \frac{2}{r^2}\frac{\partial u}{\partial \theta}\right), \tag{3}$$

$$u\frac{\partial w}{\partial r} + \frac{v}{r}\frac{\partial w}{\partial \theta} + A_w = \frac{-C}{\rho} + v\nabla^2 w, \tag{4}$$

$$u\frac{\partial T}{\partial r} + \frac{v}{r}\frac{\partial T}{\partial \theta} + w\frac{\partial T}{\partial z} = \alpha\nabla^2 T, \tag{5}$$

$$\nabla^2 \equiv \frac{\partial^2}{\partial r^2} + \frac{1}{r}\frac{\partial}{\partial r} + \frac{1}{r^2}\frac{\partial^2}{\partial \theta^2}, \tag{6}$$

where u, v, w are the velocity components in r, θ and z directions in the straight pipe, and in r, θ and φ directions in the stationary curved pipe, respectively. Also, P is the pressure, P^* the reduced pressure, C the pressure gradient in z direction, ρ the density, v the kinematic viscosity, A_u the source term in r direction, A_v the source term in θ direction, A_w the source term either in z or φ direction, α the thermal diffusion, and T the temperature. In the energy equation, Eq. (5), the dissipation energy term is neglected due to its small effect.

In the rotating straight pipe, the corresponding source terms in Eqs. (2)–(4) along with P^* and C are

$$A_u = -2\Omega w \cos\theta, \quad A_v = 2\Omega w \sin\theta,$$
$$A_w = 2\Omega(u\cos\theta - v\sin\theta), \tag{7}$$

$$P^* = P - \frac{1}{2}\rho\Omega^2(r^2\cos^2\theta + z^2), \tag{8}$$

$$C = -\frac{\partial P^*}{\partial z}, \tag{9}$$

where Ω denotes the angular velocity of rotation.

The source terms and P^* for the stationary curved pipe are

$$A_u = -\frac{w^2}{R}\cos\theta, \quad A_v = \frac{w^2}{R}\sin\theta, \quad A_w = 0, \quad P^* = P, \tag{10}$$

where R is the mean radius of curvature.

As already pointed out, the main objective of this article is the study of flow and heat transfer in stationary curved pipes and rotating straight pipes in the presence of internal fins. In this study, the fins are assumed to have negligible thickness with a symmetrical arrangement relative to the horizontal diameter of the pipe. Under these circumstances, the flow field is symmetrical, and it is enough to take into account either upper semi-circle or lower semi-circle in the numerical simulation. The boundary conditions for the velocity u, v and w are no-slip conditions on the pipe wall and on the fin surfaces:

$$u = v = w = 0 \quad \text{at } r = \frac{d}{2} \text{ and on the fin surfaces.} \tag{11}$$

Applying symmetry condition, it can be written:

$$\frac{\partial u}{\partial \theta} = \frac{\partial w}{\partial \theta} = \frac{\partial T}{\partial \theta} = 0 \quad \text{and} \quad v = 0 \quad \text{at } \theta = 0, \pi. \tag{12}$$

For pressure on the boundaries the Neumann condition is used:

$$\frac{\partial P}{\partial n} = 0. \tag{13}$$

To study heat transfer enhancement by inserting internal fins, the energy equation, Eq. (5), is solved for two

different thermal boundary conditions, i.e., constant wall temperature and constant heat flux at the wall. Therefore, the implemented thermal boundary conditions are

$$T = T_{\mathrm{w}} \text{ or } q = q_{\mathrm{w}} \quad (r = d/2 \text{ on the surface of the Finnes)} \tag{14}$$

The temperature gradient in the main flow direction under thermally fully developed condition in the constant heat flux boundary based on the average wall temperature and in the constant wall temperature boundary, respectively, are

$$\frac{\partial T}{\partial z} = \frac{\mathrm{d}T_{\mathrm{w}}}{\mathrm{d}z} = \frac{4.9 q_{\mathrm{w}}}{\rho C_p \cdot w_m \cdot d}, \tag{15}$$

$$\frac{\partial T}{\partial z} = \frac{T_{\mathrm{w}} - T}{T_{\mathrm{w}} - T_{\mathrm{b}}} \cdot \frac{\mathrm{d}T_{\mathrm{b}}}{\mathrm{d}z}, \tag{16}$$

where w_m is the average axial velocity, C_p the constant pressure heat capacity, and T_{b} the bulk fluid temperature which is defined as

$$T_{\mathrm{b}} = \frac{\int_A wT \, \mathrm{d}A}{\int_A w \, \mathrm{d}A}. \tag{17}$$

Taking into account the velocity scale of secondary flow as $U_{sR} = (\Omega w_m \cdot d)^{1/2} = w_m / R_0^{1/2}$, where $R_0 = w_m / \Omega d$ is the Rossby number, the non-dimensional parameters used in the rotating straight pipe are

$$\tilde{r} = \frac{r}{d}, \quad \tilde{w} = \frac{w}{w_m}, \quad \tilde{v} = \frac{v}{w_m} \cdot R_0^{1/2}, \quad \tilde{u} = \frac{u}{w_m} \cdot R_0^{1/2},$$

$$Re = \frac{d \cdot w_m}{v}, \quad \widetilde{P}^* = \frac{P^* \cdot R_0}{\rho \cdot w_m^2},$$

$$\widetilde{C} = \frac{d \cdot R_0^{1/2}}{\rho \cdot w_m^2} C, \quad \widetilde{T} = \frac{T_{\mathrm{w}} - T}{T_{\mathrm{w}} - T_{\mathrm{b}}} \quad \text{at } T_{\mathrm{w}} = \text{constant}, \tag{18}$$

$$\widetilde{T} = \frac{\overline{T}_{\mathrm{w}} - T}{q_{w} \cdot d/k} \quad \text{at } q_{\mathrm{w}} = \text{constant}$$

$$K_{\mathrm{LR}} = \frac{R_e}{R_0^{1/2}} = \frac{d \cdot w_m}{v \cdot R_0^{1/2}} = \frac{d \cdot U_{SR}}{v} = R_{eSR},$$

where K_{LR} denotes the Dean number in the rotating straight pipe, $\overline{T}_{\mathrm{w}}$ the average surface temperature, and k the thermal conductivity.

For the stationary curved pipe, the non-dimensional parameters can be written as

$$\tilde{r} = \frac{r}{d}, \quad \tilde{w} = \frac{w}{w_m}, \quad \tilde{v} = \frac{v}{w_m} \cdot \lambda^{1/2}, \quad \tilde{u} = \frac{u}{w_m} \cdot \lambda^{1/2},$$

$$\widetilde{T} = \frac{T_{\mathrm{w}} - T}{T_S}, \quad \widetilde{P}^* = \frac{P^* \lambda}{\rho w_m^2},$$

$$\widetilde{C} = \frac{d \cdot \lambda^{1/2}}{\rho w_m^2} C, \quad \widetilde{T} = \frac{T_{\mathrm{w}} - T}{T_{\mathrm{w}} - T_{\mathrm{b}}} \quad \text{at } T_{\mathrm{w}} = \text{constant}, \tag{19}$$

$$\widetilde{T} = \frac{\overline{T}_{\mathrm{w}} - T}{q_{w} \cdot d/k} \quad \text{at } q_{\mathrm{w}} = \text{constant},$$

$$k_{\mathrm{LC}} = \frac{R_e}{\lambda^{1/2}} = \frac{d \cdot w_m}{v \cdot \lambda^{1/2}} = \frac{d \cdot U_{SC}}{v} = R_{eCS},$$

where λ is the ratio of mean radius of curvature of the pipe to diameter of the pipe (R/d), and $U_{\mathrm{SC}} = w_m \cdot (d/R)^{1/2} = w_m / \lambda^{1/2}$ is the secondary flow velocity scale. It should be emphasized that in this study the loose coil approximation is applied, where λ is greater than 8.

In this work two set of semi-empirical formulas developed for finless stationary curved pipes and finless rotating straight pipes [19,20] are used to test the accuracy of the code implemented. For skin friction factor the semi-empirical formula proposed is

$$\frac{f}{f_0} = K_{\mathrm{L}}^{1/2}(0.0899 + 1.11 K_{\mathrm{L}}^{-0.701})$$

$$\text{for } 15 < K_{\mathrm{L}} < 3000, \ R_0 > 8, \ f_0 = \frac{64}{Re}. \tag{20}$$

Nusselt number for constant heat flux is determined by following semi-empirical formulas:

$$\frac{Nu_H}{Nu_{H0}} = 0.145 \sqrt{K_{\mathrm{L}} \sqrt{Pr}} (1 + 7.15 (K_{\mathrm{L}} \sqrt{Pr})^{-0.827})$$

$$\text{for } 0.7 \leqslant Pr \leqslant 10, \tag{21a}$$

$$\frac{Nu_H}{Nu_H} = 0.145 \sqrt{K_{\mathrm{L}} \sqrt{Pr}} (1 + 7.15 (K_{\mathrm{L}} \sqrt{Pr})^{-0.827})$$

$$\times (1 + 0.003 (K_{\mathrm{L}} \sqrt{Pr})^{0.45}) \quad \text{for } 10 < Pr < 100. \tag{21b}$$

In constant wall temperature, semi-empirical relations for Nusselt number are

$$\frac{Nu_T}{Nu_{T0}} = 0.180 \sqrt{K_{\mathrm{L}} \sqrt{Pr}} (1 + 2.72 (\sqrt{K_{\mathrm{L}} \sqrt{Pr}})^{-0.726})$$

$$\text{for } 0.7 < Pr < 10, \tag{22a}$$

$$\frac{Nu_T}{Nu_{T0}} = 0.180 \sqrt{K_{\mathrm{L}} \sqrt{Pr}} (1 + 2.72 (\sqrt{K_{\mathrm{L}} \sqrt{Pr}})^{-0.726})$$

$$\times (1 + 3 \times 10^{-5} (\sqrt{K_{\mathrm{L}} \sqrt{Pr}})^{0.9}) \quad \text{for } 10 < Pr < 100, \tag{22b}$$
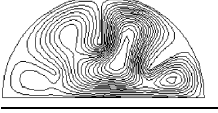
$$\frac{Nu_T}{Nu_{T0}} = 0.180 \sqrt{K_{\mathrm{L}} \sqrt{Pr}} (1 + 2.72 (\sqrt{K_{\mathrm{L}} \sqrt{Pr}})^{-0.726})$$

$$\times (1 + 0.035 (\sqrt{K_{\mathrm{L}} \sqrt{Pr}})^{0.25}) \quad \text{for } 100 < Pr < 1000. \tag{22c}$$

3. Numerical method

The governing equations, Eqs. (1)–(5), are solved by a finite volume method based on the SIMPLE algorithm. Using staggered grid, the advection–diffusion terms are discritized by power law scheme in a polar coordinate which is suitable for circular domains like in this study. For convenience, all the finite volumes are in quadrilateral shape except the one at the center, which is polygonal depending on the number of divisions used in θ-direction. The numerical results shown here are obtained in a grid with a resolution of 39×44, but the conservative property of the numerical code has been successfully tested in different

Table 1
Grid independency test for three different grid sizes

	$\dfrac{Nu_H}{Nu_{H0}}$	$\dfrac{T_w - T_m}{qd/K}$	$\dfrac{F}{F_0}$	Grid size
	5.61	0.062	3.29	29×34
	5.68	0.061	3.37	39×44
	5.74	0.0614	3.41	49×54

coarser and finer grids. The system of descritized equations are solved by TDMA method, and the relaxation techniques are applied to improve the convergency rate. It should be declared that the maximum error for the residuals in all runs is of the order of 10^{-8}.

To investigate grid independency of the code implemented, three different grid sizes as shown in Table 1 are considered to simulate a fully developed flow and heat transfer inside a curved pipe with six internal fins at constant heat flux thermal boundary conditions and Dean number of 100. The comparison of the skin friction coefficients, mean temperatures, Nusselt numbers, and flow field patterns among the three meshes indicate that the conservative property of the code is well established. The maximum difference of the values between two consecutive meshes is about 2%, which is numerically acceptable for different mesh sizes. In this study considering CPU time and the accuracy, the mesh size 39×44 is used for all the simulations.

4. Results and discussion

The numerical results presented here study and compare the six cases consisting of a finless curved pipe, a finless rotating straight pipe, internally finned stationary curved pipes with four and six fins, and internally finned rotating straight pipes with four and six fins. Unless otherwise noted, the height of fins is considered to be half of the pipe radius and the thermal boundary is constant temperature at the wall. To validate the numerical code accuracy, the following numerical results are compared with the semi-empirical relations developed by Ishigaki [19,20] for finless pipes both hydrodynamically and thermally fully developed conditions. As it will be shown, the comparison indicates good agreement with the semi-empirical results, therefore, the numerical results obtained for the internally finned pipes will be reliable.

Fig. 2a–c shows the axial velocity and secondary flow streamline contours at the three K_L numbers of 10, 100, and 800. The upper semi-circle is related to the rotating
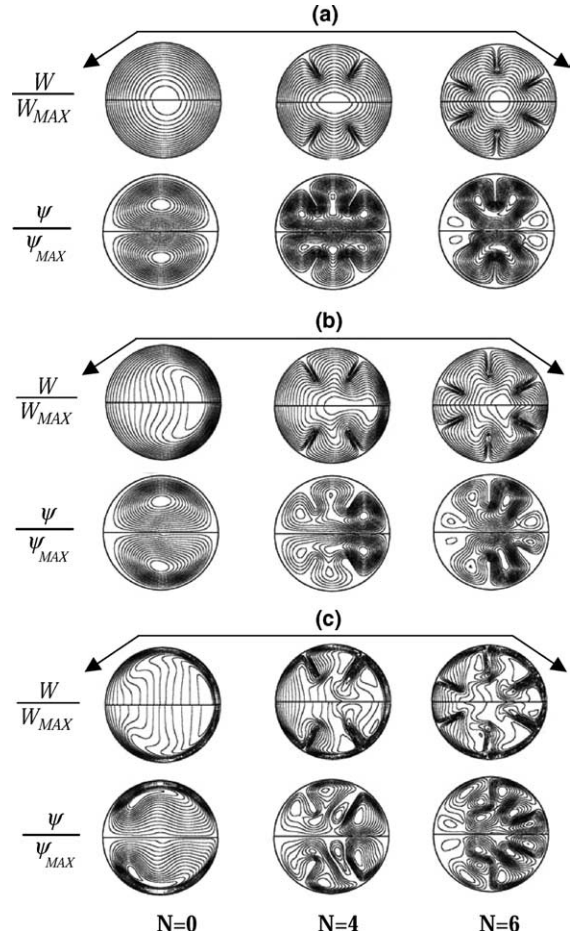

Fig. 2. Axial velocity and secondary flow streamline contours for finless pipe (left), pipe with four internal fins (middle), and pipe with six internal fins (right) at different K_L numbers. Upper semi-circle indicates rotating straight pipe and lower semi-circle indicates curved pipe. (a) $K_L = 10$, (b) $K_L = 100$, (c) $K_L = 800$.

straight pipe and the lower semi-circle is concerned with the stationary curved pipe. The results for the three cases, the finless pipe and the four and the six internally finned pipes, confirm that the analogy of flow field in both finless and internally finned pipes between a straight rotating pipe and a stationary curved pipe establishes. This has already been discovered for finless pipes by Ishigaki [19,20]. From Fig. 2b and c, it can be seen that as the K_L number increases the flow field patterns get more complex due to strong secondary flow effects.

Fig. 3a–c with the same manner mentioned in Fig. 2 represent the isothermal temperature contours at four different Prandtl numbers of 0.003, 1, 13, and 50. Here, a thermal analogy between the rotating straight pipe and the curved stationary pipe is observed, and as Prandtl number increases thermal diffusion becomes larger, especially for the internally finned pipes due to increase of heat transfer area. Also with the increase of K_L number, the temperature field patterns becomes more complex due to high intensity secondary flows.

The absolute maximum secondary stream function values, ψ_{max}, are given in Fig. 4 versus K_L numbers for finless
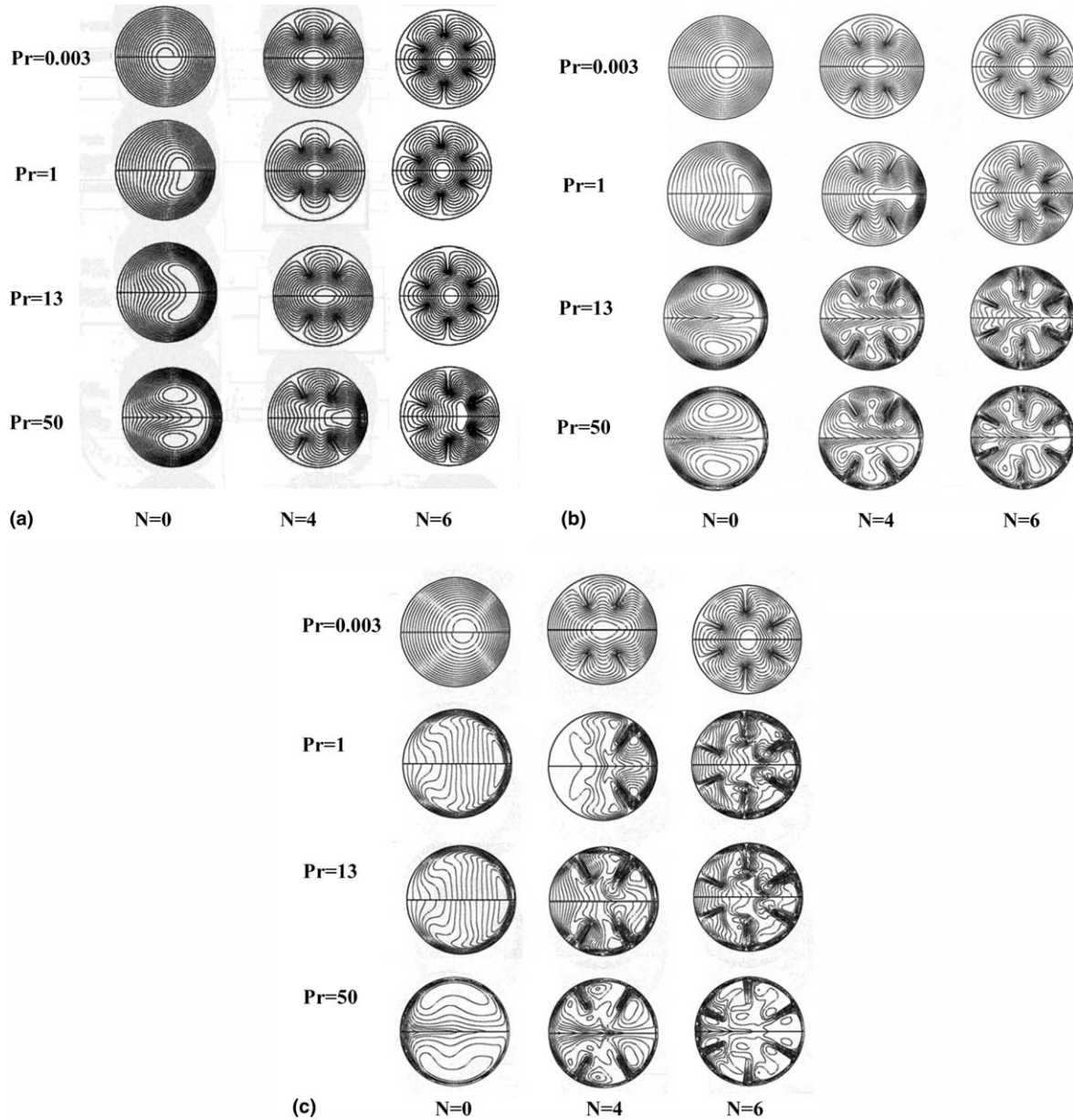
Fig. 3. Contours of temperature at different Prandtl numbers for finless pipe (left), pipe with four internal fins (middle), and pipe with six internal fins (right). (a) $K_L = 10$, (b) $K_L = 100$, (c) $K_L = 800$.
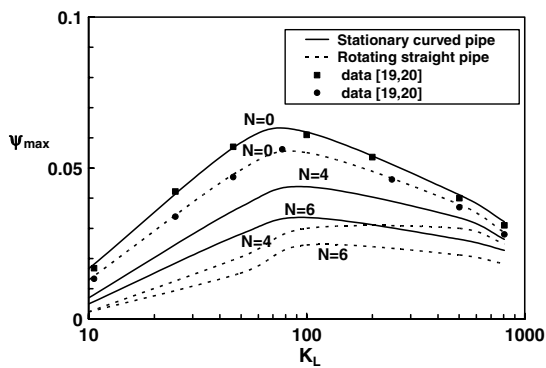

Fig. 4. Variation of maximum secondary flow stream function with K_L number for finless and internally finned rotating straight and stationary curved pipes.

and internally finned pipes. The solid lines are attributed to stationary curved pipes, dash lines are for straight rotating pipes, and the characters are for semi-empirical formula. As it can be seen from the figure, the maximum value of stream function for the stationary curved pipes in both with and without fines is greater than that of the straight rotating pipes. This is because of strong secondary flow effects in curved pipes, induced only by centrifugal forces, relative to the rotating straight pipes induced by centrifugal and coriolis forces which are not necessarily in favor of each other. Using internal fins weakens global secondary flow effect and separate it into small regions confined among the fines. Therefore, the maximum value of stream function becomes smaller in comparison with the finless cases. For the same reason, as the fin number increases,
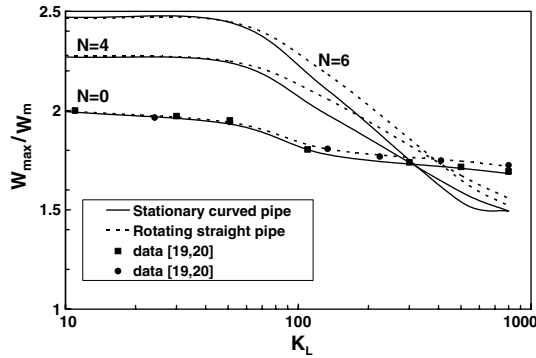
Fig. 5. Variation of maximum axial velocity with K_L for finless and internally finned rotating straight and stationary curved pipes.
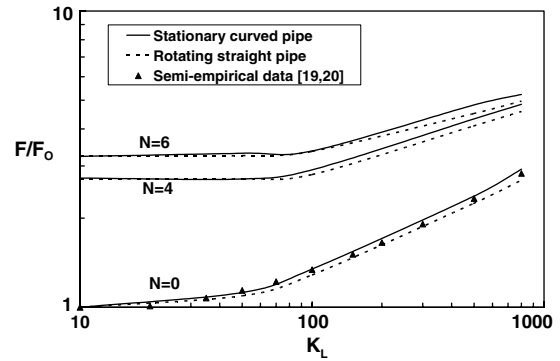

Fig. 6. Variation of friction factor with K_L number for finless and internally finned pipes.
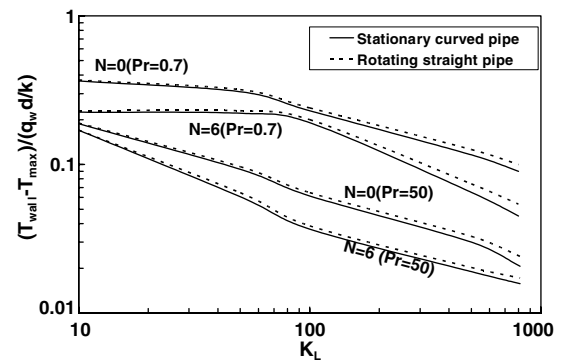

Fig. 7. Variation of maximum temperature of fluid with K_L number for finless and internally finned pipes at different Prandtl numbers.

the maximum stream function value reduces. Around K_L number of 100, the maximum point occurs, and beyond that, due to higher dissipation energy in the pipes, the secondary flow effects weaken, which result in the reduction of maximum stream function.

Fig. 5 indicates that the maximum axial velocity in fully developed region for finless pipes is smaller than that for the internally finned pipes. Here, this is because of no slip conditions applied on the fins, and as the fin numbers increases, the maximum axial velocity increases. Three different regions appear for the maximum axial velocity in Fig. 5. For K_L number less than about 50 it remains constant for all cases, and the results for stationary curved pipes in both with and without fines coincide to the same results as in rotating straight pipes. Between K_L numbers of 50 and 150, the maximum axial velocity drops more rapidly for internally finned pipes than for finless pipes, and beyond that it remains almost constant. Also, the dropping slope for the stationary curved pipes is slightly more than that of rotating straight pipes. The physical point behind this stems from the secondary flow effects, i.e. in the stationary curved pipe the higher K_L number means the higher strength of secondary flows generated by only centrifugal forces, but in a rotating straight pipe the higher K_L number indicates weaker secondary flow effects relative to the curved pipe case due to the counterbalance of centrifugal and coriolis forces. Furthermore, using internal fins strengthen secondary flow effects, and for K_L numbers greater than 300 in the stationary curved pipes and greater than 400 in the rotating straight pipes, the maximum axial velocity becomes less than the similar finless cases.

Fig. 6 shows friction factor for the six cases already mentioned. As it is evident, using internal fins increases the friction factor 2–3 times relative to the finless cases for K_L numbers less than 800, and beyond that by increasing K_L number the augmentation of friction factor decreases due to the reduction of maximum axial velocity displayed in Fig. 5. In addition, the friction factor for the K_L numbers greater than 100 in the rotating straight pipes either finless or internally finned, is slightly less than the similar stationary curved cases.

The maximum temperature versus K_L number for Prandtl numbers of 0.7 and 50 is shown in Fig. 7. Here, heating of the fluid is considered, hence, the wall temperature is greater than the fluid temperature, and therefore, the difference of the wall and the maximum fluid temperature decreases when heat transfer rate increases. Noting this point, Fig. 7 indicates that as K_L number increases the maximum temperature increases due to higher heat transfer rate induced by high intensity secondary flow effects in large K_L numbers. As it is expected, for internally fined pipes and for large Prandtl numbers, the maximum temperature is greater than the other similar cases. For the same reasons already pointed out, the maximum temperature for the stationary curved pipes is slightly greater than that for the rotating straight pipes. Fig. 8 supports the results shown in Fig. 7. Here, the variation of Nusselt number with K_L number for the same cases as in Fig. 7 at constant wall temperature is represented. For the cases shown in Fig. 8, about 20–40% enhancement in Nusselt number for the pipes with internal fins is observed. The similar results for the constant heat flux at the pipe wall are shown in Fig. 9. In Fig. 10a and b the absolute values of Nusselt numbers at two different thermal boundary conditions for stationary curved pipes and rotating straight pipes both finless and with internal fines are shown respectively. The results indicate the same trend of Nusselt number
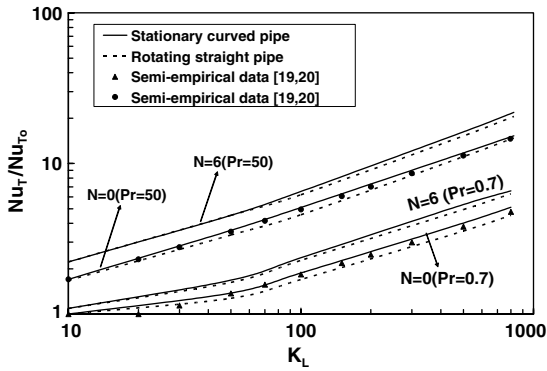
Fig. 8. Nusselt number versus K_L number in constant wall temperature for finless and internally finned pipes at different Prandtl numbers.
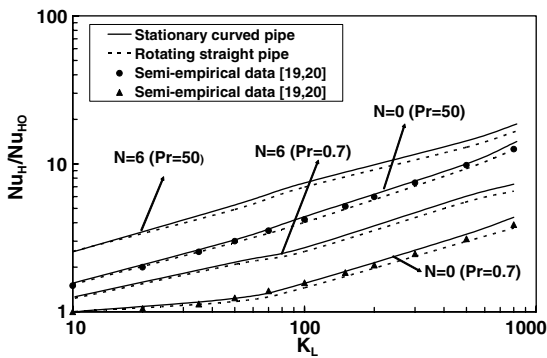

Fig. 9. Nusselt number versus K_L number in uniform heat flux at the wall for finless and internally finned rotating straight and stationary curved pipes at different Prandtl numbers.
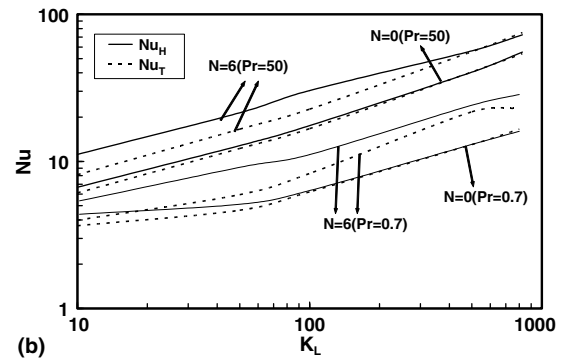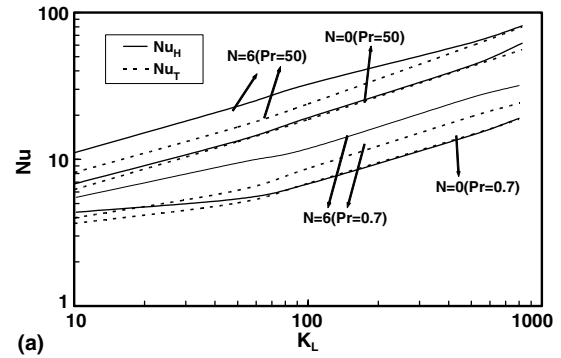

Fig. 10. Absolute Nusselt number versus K_L number in uniform heat flux and constant temperature at the wall for finless and internally finned stationary curved pipes (a) and rotating straight pipes (b) at different Prandtl numbers.
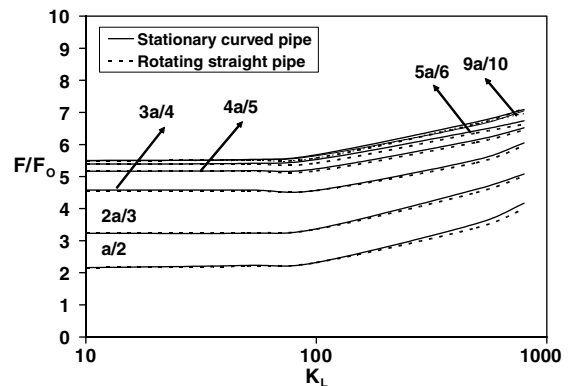

Fig. 11. Effect of fin height on friction factor at different K_L numbers for internally finned rotating straight and stationary curved pipes.

variations for the two different pipes, both quantitatively and qualitatively. Furthermore, the values of Nusselt number for the constant heat flux at the wall are greater than the ones for constant temperature at wall, especially for the pipes with internal fines.

To study the influence of fin height on the enhancement of heat transfer rate, the pipes with six internal fins for both stationary curved and rotating straight cases are considered. Seven different fin heights, starting from one third to nine tenth of the pipe radius, are selected. In Fig. 11, the friction factor for seven different fin heights is shown versus K_L number. It can be realized that the increase rate of friction factor due to fin height becomes smaller as the fin height increases. For the corresponding cases, Nusselt number variations with K_L number for the constant heat flux at the wall are shown in Fig. 12. To find out the optimum fin height, Coulburn factor ($j = Nu/(RePr^{1/3})$) over Fanning friction factor versus K_L number is shown in Fig. 13a and b for different fin sizes. For K_L numbers less than 100 (Fig. 13a), the J/F values for fin height equal to 0.8 of pipe radius are greater than the other cases, indicating the optimum fin height to heat transfer enhancement. But for K_L numbers greater than 100, an interesting result takes place. In this case, it can be realized from Fig. 13b, as the fin height reduces the J/F values increases. Therefore,

insertion of internal longitudinal fins for K_L numbers greater than 100 results in consuming greater pump power to overcome friction, and there is no optimum value for fin height in this range.

Consequently, the optimum fin height, taking into account the heat transfer enhancement and the drawback of friction factor increase, is 0.8 of pipe radius for K_L numbers less than 100. By considering this optimum value, the heat transfer rate in internally finned curved pipes and straight rotating pipes increase about 6 times compared to the corresponding finless pipes.
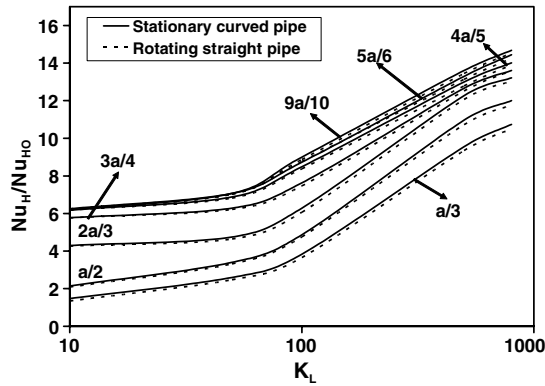
Fig. 12. Effect of fin height on Nusselt number at different K_L numbers for internally finned rotating straight and stationary curved pipes.
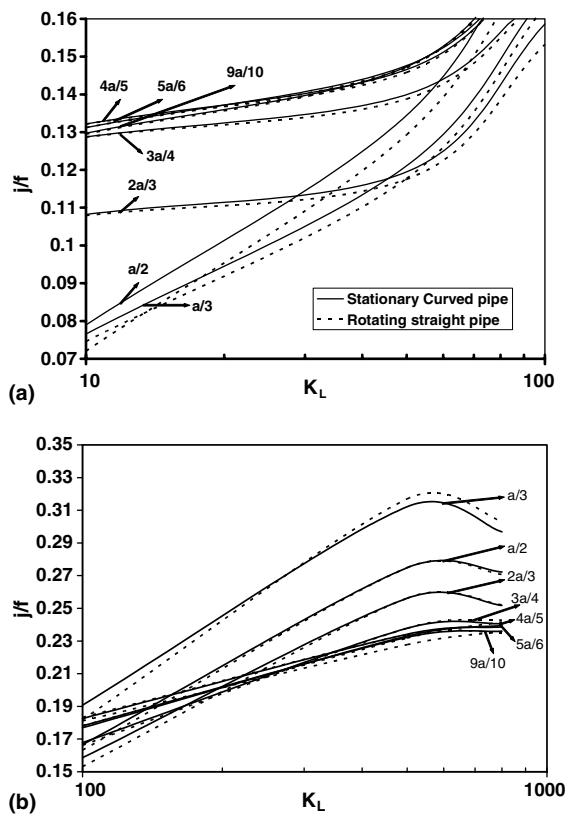

Fig. 13. Colburn factor over Fanning friction factor (j/f) versus Dean number (K_L). (a) For K_L less than 100 and (b) for K_L greater than 100.

For the next studies, this work can be extended for flows inside curved and rotating pipes with longitudinal internal fins and also rectangular cross sections to take into account cooling problems in rotating machines such as gas turbine blades. Among the papers in this regard for finless pipes, it may be referred to the work of Zhang et al. [21] who studied Fluid flow in a finless rotating curved rectangular duct. Furthermore, another interesting phenomenon concerning with the effects of chaotic aspects on flow and heat transfer can be studied in internally finned curved pipes as Mokrani

et al. [22] and Lemenand and Peerhossaini [23] have carried out for finless pipes.

5. Conclusions

Laminar incompressible viscous flow in internally finned curved pipes and rotating straight pipes are studied in both hydrodynamically and thermally fully developed conditions. The numerical analysis indicates that the analogy of flow field between curved pipes and rotating straight pipes in the presence of internal fins still occur as that of for finless pipes. The presence of internal fins causes the secondary flows separate into small regions among the fins with more vortices relative to the finless cases. The effects of Dean number (K_L) versus friction factor, Nusselt number, and other non-dimensional parameters are studied in detail. From the numerical results obtained, an optimum fin height about 0.8 of pipe radius is determined for Dean numbers less than 100. At this optimum value, the heat transfer coefficient appears to be 6 times as that of finless pipes. For K_L numbers greater than 100 there is no optimum fin height concerning heat transfer enhancement without drawback of friction power.

References

[1] K. Nandakumar, J.A. Masliyah, Fully developed viscous flow in internally finned tubes, Chem. Eng. J. 10 (1975) 113–120.

[2] H.M. Soliman, A. Feingold, Analysis of fully developed laminar flow in longitudinal internally finned tubes, Chem. Eng. J. 14 (1977) 119–128.

[3] H.M. Soliman, T.S. Chau, A.C. Trupp, Analysis of laminar heat transfer in internally finned tubes with uniform outside wall temperature, ASME J. Heat Transfer 102 (1980) 598–604.

[4] J.H. Masliyah, K. Nandakumar, Heat transfer in internally finned tubes, ASME J. Heat Transfer 98 (1976) 257–261.

[5] H. Hu, Y.P. Chang, Optimization of finned tubes for feat transfer in laminar flow, ASME J. Heat Transfer 95 (1973) 332–338.

[6] I.M. Rustum, H.M. Soliman, Numerical analysis of laminar forced convection in the entrance region of tubes with longitudinal internal fins, ASME J. Heat Transfer 110 (1988) 310–313.

[7] C. Prakash, Y.D. Liu, Analysis of laminar flow and heat transfer in the entrance region of an internally finned circular duct, ASME J. Heat Transfer 107 (1985) 84–91.

[8] C. Prakash, S.V. Patankar, Combined free and forced convection in vertical tubes with radial internal fins, ASME J. Heat Transfer 103 (1981) 566–572.

[9] Z.F. Dong, M.A. Ebadian, Convective and radiative heat transfer in the entrance region of an elliptic duct with fins, Numer. Heat Transfer 21 (1992) 91–107.

[10] Z.F. Dong, M.A. Ebadian, A numerical analysis of thermally developing flow in elliptic ducts with internal fins, Int. J. Heat Mass Transfer 12 (2) (1991) 166–172.

[11] A. Campo, J. Chang, Correlation equations for friction factors and convective coefficients in tubes containing bundles of internal, longitudinal fins, Heat Mass Transfer 33 (1997) 225–232.

[12] G. Fabbir, Heat transfer optimization in internally finned tubes under laminar flow conditions, Int. J. Heat Mass Transfer 41 (10) (1998) 1243–1253.

[13] M. Huq, A.M. Aziz-ul Huq, M.M. Rahman, Experimental measurements of heat transfer in an internally finned tube, Int. Commun. Heat Mass Transfer 25 (5) (1998) 619–630.

[14] G.A. Ledezma, A. Campo, Computation of the Nusselt number asymptotes for laminar forced convection flows in internally finned tubes, Int. Commun. Heat Mass Transfer 26 (3) (1999) 399–409.

[15] B. Yu, J.H. Nie, Q.W. Wang, W.Q. Tao, Experimental study on the pressure drop and heat transfer characteristics of tubes with internal wave-like longitudinal fins, Heat Mass Transfer 35 (1999) 65–73.

[16] Y.Y. Tsui, S.W. Leu, Heat transfer enhancement by a multilobe vortex generator in internally finned tubes, Numer. Heat Transfer Part A 35 (1999) 553–566.

[17] V.D. Sakalis, P.M. Hatzikonstantinou, Laminar heat transfer in the entrance region of internally finned square ducts, ASME J. Heat Transfer 123 (2001) 1030–1034.

[18] O. Zeitoun, A.S. Hegazy, Heat transfer for laminar flow in internally finned pipes with different fin heights and uniform wall temperature, Heat Mass Transfer 40 (2004) 253–259.

[19] H. Ishigaki, Analogy between laminar flows in curved pipes and orthogonally rotating pipes, J. Fluid Mech. 268 (1994) 133–145.

[20] H. Ishigaki, Analogy of forced convective heat transfer between laminar flows in curved pipes and orthogonally rotating pipes, JSME Int. J. Ser. B 42 (1) (1999) 48–55.

[21] J. Zhang, B. Zhang, J. Jü, Fluid flow in a rotating curved rectangular duct, Int. J. Heat Fluid Flow 22 (2001) 583–592.

[22] A. Mokrani, C. Castelain, H. Peerhossaini, The effects of chaotic advection on heat transfer, Int. J. Heat Mass Transfer 40 (13) (1997) 3089–3104.

[23] T. Lemenand, H. Peerhossaini, A thermal model for prediction of the Nusselt number in a pipe with chaotic flow, Appl. Thermal Eng. 22 (15) (2002) 1717–1730.